Chemical Engineering Journal 382 (2020) 122879

Contents lists available at ScienceDirect

Chemical Engineering Journal

journal homepage: www.elsevier.com/locate/cej

Calcium carbonate granulation in a fluidized-bed reactor: Kinetic, parametric and granule characterization analyses

Arianne S. Sioson[a], Angelo Earvin Sy Choi[b], Mark Daniel G. de Luna[a,c,*], Yao-Hui Huang[d], Ming-Chun Lu[e,*]

[a] Environmental Engineering Program, National Graduate School of Engineering, University of the Philippines Diliman, Quezon City 1101, Philippines
[b] National Research Center for Disaster-Free and Safe Ocean City, Busan 49315, Republic of Korea
[c] Department of Chemical Engineering, University of the Philippines Diliman, Quezon City 1101, Philippines
[d] Department of Chemical Engineering, National Cheng Kung University, Tainan 70101, Taiwan
[e] Department of Environmental Resources Management, Chia Nan University of Pharmacy and Science, Tainan 71710, Taiwan

HIGHLIGHTS

- Carbon dioxide capture, utilization and storage in the form of calcium carbonate.
- Calcium carbonate homogeneous granulation in a fluidized-bed reactor.
- The kinetic analysis revealed that the pseudo-second order best fitted the results.
- Calcium-is-to-carbonate molar ratio directly affects the granule characteristics.
- High purity of calcium carbonate-aragonite granules were produced.

GRAPHICAL ABSTRACT

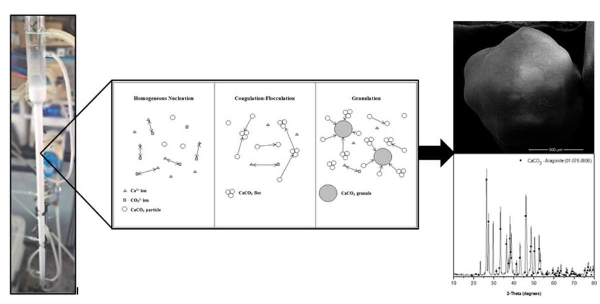

ARTICLE INFO

Keywords:
Calcium carbonate
Carbon dioxide capture
Fluidized-bed reactor
Global warming
Homogeneous granulation
Kinetic analysis

ABSTRACT

The granulation of calcium carbonate ($CaCO_3$) exhibited high industrial demand due to its wider application and importance in cement, paper, glass and steel manufacturing. This paper investigated the granulation kinetics of $CaCO_3$ through the fluidized-bed homogeneous granulation (FBHG) process during the homogenous nucleation stage. The CaOH solution was used as source of Ca^{2+} reactant, while K_2CO_3 solution as source of CO_3^{2-} precipitant. The mechanism followed the pseudo-second order kinetics. The calcium cation attracts the carbonate anion to form $CaCO_3$ through a double displacement chemical reaction. The calcium-is-to-carbonate molar ratio ($[Ca^{2+}]/[CO_3^{2-}]$) was varied into 1.25 to 2.50, with constant values of pH = 10 ± 0.2, influent carbonate concentration = 10 mM and total influx flow rate = 60 mL min^{-1}. The ideal $[Ca^{2+}]/[CO_3^{2-}]$ condition was found to be at 1.50 that means the precipitation of $CaCO_3$ grew and stayed inside the reactor. At the same condition, granules of diameter size of 1 mm to 2 mm were collected with a subrounded shape and smooth surface as shown by its surface morphology. The characterization analysis also verified the high purity of $CaCO_3$-aragonite granules precipitated through the FBHG process.

* Corresponding authors at: Department of Chemical Engineering, University of the Philippines Diliman, Quezon City 1101, Philippines (M.D.G. de Luna) and Department of Environmental Resources Management, Chia Nan University of Pharmacy and Science, Tainan 71710, Taiwan (M.-C. Lu).

E-mail addresses: ariannesiosondost10@gmail.com (A.S. Sioson), angelochoi2003@yahoo.com (A.E.S. Choi), mgdeluna@up.edu.ph (M.D.G. de Luna), mmclu@mail.cnu.edu.tw (M.-C. Lu).

https://doi.org/10.1016/j.cej.2019.122879
Received 25 June 2019; Received in revised form 30 August 2019; Accepted 17 September 2019
Available online 18 September 2019
1385-8947/

1. Introduction

In industries, calcium carbonate ($CaCO_3$) is largely used as an important material in cement, paper, glass and steel manufacturing. The conventional industrial processes of precipitating $CaCO_3$ are through the lime soda process and carbonation process [1,2]. In the lime soda process, calcium hydroxide ($Ca(OH)_2$) is reacted with sodium carbonate (Na_2CO_3) to precipitate $CaCO_3$. In the carbonation process, crushed limestone is burned to decompose quicklime and carbon dioxide (CO_2), where the quicklime is transformed into slake lime slurry by the addition of water, and then $CaCO_3$ is formed by reacting the slurry with pressurized CO_2. In comparison, the major objective of the lime soda process is the recovery of sodium hydroxide (NaOH) making the precipitated $CaCO_3$ as a secondary by-product; while in the carbonation process, longer steps and high energy are required.

Another promising method of precipitating a high purity $CaCO_3$ is through the fluidized-bed homogeneous granulation (FBHG) process using a fluidized-bed reactor (FBR). Fluidized-bed technology has been widely used in pharmaceutical and fertilizer manufacturing, as well as in wastewater treatment. Related studies used FBR for water softening, nutrient removal and heavy metal recovery through heterogeneous or homogeneous granulation processes [3,4]. In heterogeneous granulation, seed materials are added inside the reactor. This serves as the nuclei that forms particles through a homogeneous nucleation. On the other hand, the nucleus in the homogeneous granulation process is formed by homogeneous nucleation and coagulation-flocculation, in which the flocs would later agglomerate and grow through granulation [5]. Since $CaCO_3$ can be easily precipitated, the use of the FBHG process has the following advantages: it requires less chemical input, has higher removal and granulation efficiencies, produces no sludge, and precipitates high purity granules [6,7]. In recent years, the FBHG process has been used for the treatment of various pollutants such as aluminum [8], calcium [9,10], copper [11], lead [5], nickel [12], oxalate [13], phosphate [14] and zinc [15]. However, the application of the FBHG process in converting the captured CO_2 (in the form of potassium carbonate (K_2CO_3)) to $CaCO_3$ has never been investigated. This is specifically important in the aspect of carbon capture, utilization and storage as it have recently drawn greater scientific interest due to the utilization of the captured CO_2 into algae cultivation, concrete curing, polymer production, and mineral carbonation [16]. Thus, the conversion of K_2CO_3 in a $CaCO_3$ homogeneous granulation setup is essential to examine the results of its possible applicability in future works.

Kinetic studies in the aspect of fluidized-bed modelling have been investigated in the settings of the FBR [17], slurry bubble column reactor [18], tubular fixed-bed quartz reactor [19], tubular flow reactor [20] and fixed-bed multi-tubular reactor [21]. However, the kinetics of $CaCO_3$ granulation have not yet been explored in a FBHG setup. Moreover, there are still other factors that need to be examined in the system with regards to the effect on the molecular processes such as physisorption and/or chemisorption interaction, and diffusion of particles [22,23]. Thus, the kinetics of $CaCO_3$ homogeneous granulation in a FBR were considered in order to determine the best model to describe the reaction mechanism.

In this work, the influence of calcium dose as precipitant in the kinetics during homogeneous nucleation of $CaCO_3$ precipitation by FBHG process has been investigated. Calcium precipitant dose or calcium-is-to-carbonate molar ratio ($[Ca^{2+}]/[CO_3^{2-}]$) as a set parameter was varied to determine the most economical calcium precipitant input with high removal efficiencies and good quality granule production. Other essential conditions such as operating pH, influent carbonate concentration ($[CO_3^{2-}]_{in}$) and total influx flow rate (Q_T) were maintained into constant values of 10 ± 0.2, 10 mM and 60 mL min^{-1}, respectively. The precipitated $CaCO_3$ granules in the experimental runs were also collected, air-dried and sieved for further physical and chemical characterization in its surface morphology, crystalline composition and elemental composition.

2. Materials and methods

2.1. Chemicals

The chemicals and reagents used in this research were of analytical grade with no further purification. Potassium carbonate (K_2CO_3: 99.5% purity, New Star Instrument, Taiwan) and calcium hydroxide ($Ca(OH)_2$: 90% purity, New Star Instrument, Taiwan) solutions, as influent carbonate and precipitant calcium sources, respectively, were prepared by dissolving separately the K_2CO_3 and $Ca(OH)_2$ in reverse osmosis (RO) water from the RODA ultrapure water system (resistance of 18.2 MΩ) with their specific constant concentrations. The solution pHs of the $Ca(OH)_2$ solutions were set at 8 ± 0.05 while the K_2CO_3 solutions were set at an operating pH of 10 ± 0.2 using sodium hydroxide (NaOH: Formosa Plastic Corporation, Taiwan) and nitric acid (HNO_3: 70% purity, New Star Instrument, Taiwan). Reagents used for alkalinity test were N/50 sulfuric acid (H_2SO_4: 95–98%, PanReac AppliChem) as a titrant, 1% phenolphthalein solution (Phenolphthalein, New Star Instrument, Taiwan) as an indicator phenolphthalein alkalinity, and 0.1% methyl orange (Methyl orange, Riedel-de Haën) as an indicator for the total alkalinity.

2.2. Fluidized-bed reactor

The $CaCO_3$ homogeneous granulation was done in a laboratory-scale FBR as shown in Fig. 1. The advantages of the fluidized-bed granulation include a minimal chemical dosage condition, less space requirement and generates low moisture content in its granules [12].

The processes of treatment and recovery were somehow similar to that of the conventional precipitation method. By dosing the right amounts of carbonate and calcium ions inside the reactor, granule products are formed through a chemical reaction. Usually, seeds such as silica or sand are first injected into the reactor, which serves as the nuclei of the forming granules. The grains, then would increase in diameter and removed after. However, using a seeding material produces low sludge quality and high water content in its granules that make the recovery of pure material difficult [3,24]. Thus, the rise of the developments in the FBHG process that do not require a seeding step. In

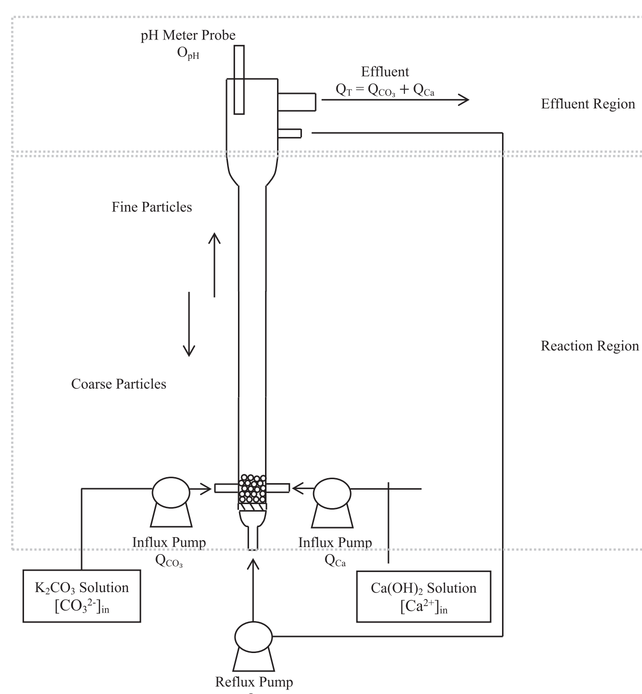

Fig. 1. Schematic setup of the fluidized-bed reactor.

the homogeneous process, the influent with the reactant makes contact with the precipitant; it collects an adequate amount of active sites that in turn generates the homogeneous granules. Afterwards, particle growth and nucleation occur that yield towards large masses of high-purity granule particles [5,25].

The cylindrical Pyrex glass reactor with a total volume of 550 mL was divided into two parts as shown in Fig. 1 [5]. The upper part which was the effluent region has the dimensions of 4 cm for its inner diameter and 15 cm for its height. The sudden expansion in this part provided more area for granules inside the reactor and decreased upflow velocity, thus prevented fine particles to be drained out. The lower part which was the reaction region has dimensions of 2 cm in inner diameter and 80 cm in height. This particular region where granulation occurred has three inlets in the bottom section. The two horizontal inlets were for the reactant and precipitant, while the vertical inlet was for the effluent recirculation. The glass beads inside the reactor were necessary to support the granulation bed, to avoid bubble formation and clogging, and to distribute uniformly the liquid solution flow inside the reactor from the three inlets.

2.3. CO_2 absorption and granulation

The main idea of the research was two-stage CO_2 emissions capture using a potassium hydroxide (KOH) solution as the absorbent, and CO_2 conversion in the form of $CaCO_3$ granules. The chemical reactions that best describe the series reaction in the two-stage system of CO_2 absorption and granulation is shown in Eqs. (1) and (2), respectively.

$$KOH(aq) + CO_2(g) \rightarrow K_2CO_3(aq) + H_2O \tag{1}$$

$$K_2CO_3(aq) + Ca(OH)_2(aq) \rightarrow CaCO_3(s) + KOH(aq) \tag{2}$$

Since KOH absorption of CO_2 gas has been widely explored such as in the studies of Smirnova et al. [26] and Yoo et al. [27], it was found out that it has a high capture capacity. Therefore, this was not included in this research. Instead of a simple carbon capture and storage, a new demand for research on the conversion of CO_2 into a more valuable product emerged. Thus, this research paper is primarily focused on the second stage of the proposed carbon capture, utilization and storage, which is the $CaCO_3$ homogeneous granulation in the FBR. A synthetic K_2CO_3 solution was used as CO_2 source in its carbonate form.

2.4. Experimental procedure

The reactor was initially loaded with glass beads of the same size up to 1 cm above the horizontal inlets which would uniformly distribute the hydraulic load and then filled with 450 mL RO water up to the effluent outlet to avoid bubbling. Granulation of $CaCO_3$ into granules was initiated by controlling the parameters, operating pH to 10 ± 0.2, $[CO_3^{2-}]_{in}$ to 10 mM, and Q_T to 60 mL min^{-1}. The reflux flow rate (Q_R) was set at 30 mL min^{-1} at the beginning and then increased by 10 mL min^{-1} every 12 h after 24 h until 100 mL min^{-1} was reached. To determine the kinetics of granulation during the homogeneous nucleation at different calcium precipitant dosage, the $[Ca^{2+}]/[CO_3^{2-}]$ ratios were varied into 1.25, 1.50, 1.75, 2.00, 2.25 and 2.50 and a $Ca(OH)_2$ stock solution pH setting of 8 ± 0.05. These were considered because it was found out that the saturation of the solution with respect to concentration of Ca^{2+} and CO_3^{2-}, is the dominant factor influencing $CaCO_3$ granulation [1,10]. The pH was controlled by adding NaOH and HNO_3 in the stock solutions of K_2CO_3 and $Ca(OH)_2$ [28]. The pH was examined using a pH meter/ORP controller PC-310 from Shin Shiang Tech Instruments. The process followed the homogeneous granulation process which does not require the addition of seed materials. In the homogeneous process, the influent with the reactant makes contact with the precipitant; it collects sufficient active sites that bring about the formation of high-purity homogeneous granules through nucleation and particle growth [5,25].

Every variation of $[Ca^{2+}]/[CO_3^{2-}]$ lasted up to 168 h with sampling done every 2 h on the first 20 h, and then once every 24 h. Sampling was done by collecting two 100 mL water sample from the effluent using 25 mL syringe with one filtered with a 0.45 μm micro-syringe filter. The two samples were then analyzed to calculate the $[Carbonate]_R$ and $[Carbonate]_G$ in Eqs. (3) and (4), respectively. The $[Carbonate]_R$ was used to evaluate the total carbonate concentration that was precipitated, while $[Carbonate]_G$ was used to determine whether the carbonate precipitated forms into granules or into sludge. Moreover, the carbonate granules weight fraction ($[Carbonate]_{WF}$) was quantified using Eq. (5). The removal was evaluated to prove the capability of the FBR to precipitate and recover carbonate in its granule form by determining the residuals in the effluent, while the granulation efficiency was evaluated to prove that the granules formed were of low water content and less or no sludge was produced.

$$[Carbonate]_R, \% = \left(1 - \frac{[Carbonate]_d \times Q_T}{[CO_3^{2-}]_{in} \times Q_{CO_3}}\right) \times 100 \tag{3}$$

$$[Carbonate]_G, \% = \left(1 - \frac{[Carbonate]_t \times Q_T}{[CO_3^{2-}]_{in} \times Q_{CO_3}}\right) \times 100 \tag{4}$$

$$[Carbonate]_{WF}, \% \text{ (every mesh size)} = \frac{W_{ms}}{W_t} \times 100 \tag{5}$$

where Q_T is the sum of carbonate influx flow rate (Q_{CO_3}, mL min^{-1}) and calcium influx flow rate (Q_{Ca}, mL min^{-1}), $[Carbonate]_d$ is the dissolved effluent carbonate concentration (mM), $[Carbonate]_t$ is the total effluent carbonate concentration (mM), W_{ms} is the weight of granules collected in every mesh size (g), and W_t is the total weight of the granules collected (g).

After every experimental run, the granules formed were collected, air-dried, sieved and analyzed for particle size distribution, surface morphology, molecular structure and elemental composition.

2.5. Analytical methods and granules characterization

The concentrations of dissolved and total effluent carbonate were analyzed using Hach Method 8221 – Phenolphthalein and Total Alkalinity Buret Titration, the standard methods for the examination of water and wastewater 2320 B for United States Environmental Protection Agency – National Pollutant Discharge Elimination System (USEPA NPDES). Bicarbonate, carbonate and hydroxide alkalinity were calculated using phenolphthalein and total alkalinity, then bicarbonate and carbonate alkalinity were used as a source of the final carbonate concentration of dissolved and total effluent carbonate.

The particle size distribution of the granules collected in every operating pH was determined using a sieve analysis, with sieves opening diameters of 2 mm, 1 mm, 0.59 mm, 0.42 mm and 0.149 mm. The total weight and the weight in each size fraction were recorded, and these were used in calculating the percentage of each size fraction.

The biggest granules in every $[Ca^{2+}]/[CO_3^{2-}]$ were analyzed for its physical and chemical characterization. The surface morphology was visualized using the Scanning Electron Microscope (SEM, FEI Quanta 200 Environmental Scanning Electron Microscope), the structural and molecular formula of the granules were determined by an X-ray Diffraction (XRD, Multi-function X-ray Diffractometer), and elemental composition was examined by Energy Dispersive X-ray (EDX) spectroscopy.

2.6. Kinetic models

The homogeneous nucleation kinetics of $CaCO_3$ in the FBR at different calcium precipitant dosages were studied to determine the rate of chemical reaction occurred and the factors that could affect its rate. The granulation of $CaCO_3$ is generally described by the nucleation and agglomeration mechanisms. Nucleation is expected to occur through the

Table 1
Pseudo kinetic models and the forms used in this study.

Kinetic model	Equation	Linear form	Plot
Pseudo first order	$\frac{dq_t}{dt} = k_1(q_e - q_t)$	$\log(q_e - q_t) = \log(q_e) - \frac{k_1 t}{2.303}$	$\log(q_e - q_t)$vst
Pseudo second order	$\frac{dq_t}{dt} = k_2(q_e - q_t)^2$	$\frac{t}{q_t} = \frac{1}{k_2 q_e^2} + \frac{1}{q_e}t$	$\frac{t}{q_t}$vst

double displacement chemical reaction by the attraction of Ca^{2+} and $CO_3{}^{2-}$ ions to form a particle of $CaCO_3$. However, the agglomeration and growth of the granule could occur both or either through the nucleation of new particle at the surface or through the particle agglomeration by physical attraction. The investigation of the mechanism of $CaCO_3$ granulation through the FBHG process was done in terms of the PFO and PSO linear forms. The PFO describes the physical interaction between particles, while the PSO describes the chemical interaction between ions that results to the nucleation and granule growth. The critical part of $CaCO_3$ granulation usually occurs during homogeneous nucleation, thus, the kinetic study during this stage was considered. The experiments of the kinetic models were conducted at pH of 10 ± 0.2, $[CO_3{}^{2-}]_{in}$ of 10 mM, Q_T of 60 mL min^{-1} and at varying $[Ca^{2+}]/[CO_3{}^{2-}]$ of 1.25, 1.50, 1.75, 2.00, 2.25 and 2.50, with sampling done at every 2 h for the first 20 h and at its succeeding 24 h intervals. For the kinetic models of the PFO and PSO equations, the linear forms and plots are shown in Table 1 with the parameters q_e (mg g^{-1}) as the equilibrium nucleation capacity, h (mg g^{-1} h^{-1}) as initial nucleation rate, and k_1 (h^{-1}) and k_2 (g mg^{-1} h^{-1}) as its rate constants, calculated using Eqs. (6)–(9), respectively [29].

$$q_e = \frac{1}{slope} \tag{6}$$

$$h = kq_e^2 \tag{7}$$

$$k_1 = -2.303 \times slope \tag{8}$$

$$k_2 = \frac{slope^2}{intercept} \tag{9}$$

3. Results and discussion

3.1. Kinetics of $CaCO_3$ granulation at homogeneous nucleation

In relation to the carbon capture technologies, various processes in past studies with their corresponding results in its kinetic parameters are listed in Table 2 [22,30–33]. Different processes of CO_2 capture had different mechanisms and kinetic reaction models. Since no study has yet to focus on the subsequent conversion of K_2CO_3 (as CO_2 source) in the form of $CaCO_3$, the kinetics of $CaCO_3$ homogeneous granulation in a FBR were considered in order to determine the best model to describe the reaction mechanism. The granulation kinetics of $CaCO_3$ were analyzed using the PFO model by plotting $\log(q_e - q_t)$ versus time (h), where q_e and q_t were the amount granulated inside FBR in equilibrium and in a specified time, respectively. The calculated parameters shown in Table 3, with their corresponding correlation coefficients (R^2) in the range of 0.817 to 0.953, were obtained from the slope and intercept of its generated linear forms. Since the R^2 values obtained in PFO model were found to be much lower than 1, the model was considered not suitable to appropriately describe the reaction kinetics [34].

Table 3
Parameters calculated in the pseudo-first and pseudo-second order kinetic models for $CaCO_3$ precipitation through the FBHG process.

$[Ca^{2+}]/[CO_3{}^{2-}]$	PFO			PSO			
	k_1	q_e	R^2	k_2	q_e	h	R^2
1.25	0.0031	1.149	0.953	0.661	1.260	1.539	0.9991
1.50	0.0016	1.240	0.923	1.450	1.371	2.723	0.9986
1.75	0.0014	1.330	0.817	2.293	1.435	4.929	0.9999
2.00	0.0011	1.554	0.893	2.515	1.651	6.859	0.9999
2.25	0.0008	1.674	0.941	2.641	1.753	9.042	0.9999
2.50	0.0009	1.897	0.911	2.482	1.991	9.843	0.9999

The granulation kinetics of $CaCO_3$ in FBR were also analyzed using the PSO model by plotting t/q_t versus time (h). The calculated parameters and R^2 values were also presented in Table 3. The R^2 values were found to be greater than 0.99 in all the varied $[Ca^{2+}]/[CO_3{}^{2-}]$ conditions. The results indicated that the PSO kinetics were the fitted model that could best describe the $CaCO_3$ granulation kinetics through the FBHG process [35]. The plot of PSO model yielded a linear line as illustrated in Fig. 2. The granulation kinetics fitted in the PSO model implies that the mechanism relies on the assumption of the occurrence of chemical sorption leading towards nucleation and granulation. Chemisorption describes the ion exchange reaction involving the valency forces through the sharing or exchange of electrons between particles as covalent forces [36]. The calcium cation attracts the carbonate anion that forms the particle of $CaCO_3$ through the double displacement chemical reaction, and the particle attracts towards other particle or surface by forming chemical bonds. PSO is applicable at a higher concentration. This means the lower the concentration, the lower the collision of ions. This in turn makes the precipitation of $CaCO_3$ slower [9].

As depicted in Fig. 2(a), the steep slopes refer to a larger growth rate constant and a faster growth. The steepest slope was found to be at $[Ca^{2+}]/[CO_3{}^{2-}]$ of 1.50, which also obtained the highest weight fraction of the bigger sized granules based on a sieve analysis and the particle size distribution trend. A further decreased and increased in the $[Ca^{2+}]/[CO_3{}^{2-}]$ of 1.50 resulted to lower growth rate. The result of the linear relationship of h and q_e with respect to the $[Ca^{2+}]/[CO_3{}^{2-}]$ is shown in Fig. 2(b). There were high initial nucleation rates during the first few hours of the experiment during homogeneous nucleation, and throughout the experiment reached an equilibrium nucleation capacity, which increased when the $[Ca^{2+}]/[CO_3{}^{2-}]$ were also increased. A high initial nucleation rate was expected due to an unseeded granulation process (homogeneous nucleation) that forms the nuclei of new small granules. This was the dominant mechanism in the first few hours in order to produce granules. When there were enough granules inside the reactor, the nucleation rate decreases due to the particles that shifts into an agglomeration step to form bigger granules.

The equilibrium reactions of the $CaCO_3$ system reaction network are

Table 2
Comparison of kinetic studies in the aspect of carbon capture technologies.

Process	Fitted kinetic model	Rate constant	Reference
• Alkanolamines absorption	PSO	0.11 to 3.67 m^3 mol^{-1} s^{-1}	[31]
• Adsorption on KOH N-enriched activated carbon	Fractional order	0.07 to 0.43 min^{-1}	[32]
• Adsorption on oxygen enriched porous carbon monoliths	Fractional order	0.92 to 13.85 min^{-1}	[33]
• Adsorption on solid amine-functionalized sorbents	Avrami's model	0.0535 to 0.0762 s^{-1}	[19]
• Absorption into 1-(2-hydroxyethyl)pyrrolidine solvent	PFO	11.34 to 136.35 s^{-1}	[34]

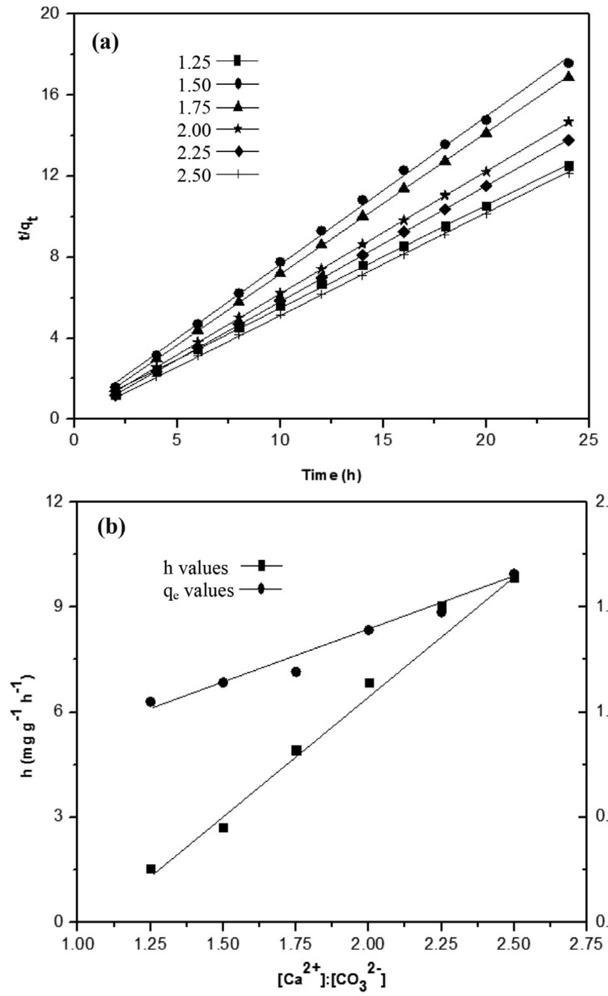

Fig. 2. (a) Pseudo second order kinetics by a linear method in the precipitation of $CaCO_3$ through the FBHG process at varying $[Ca^{2+}]/[CO_3{}^{2-}]$ levels and (b) its corresponding h and q_e values.

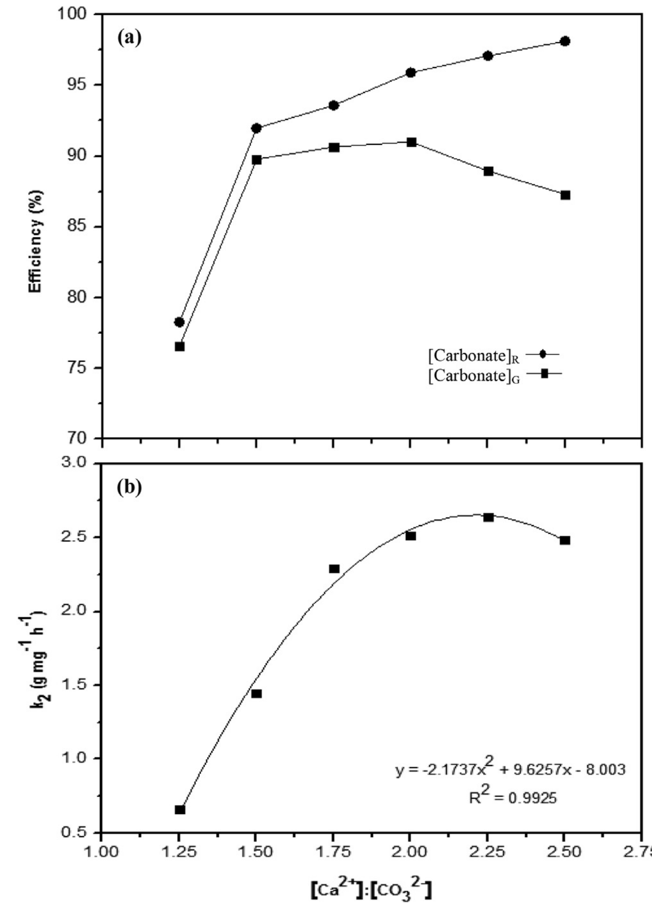

Fig. 3. (a) Average of $[Carbonate]_R$ —●— and $[Carbonate]_G$ —■— at varying $[Ca^{2+}]/[CO_3{}^{2-}]$ conditions and (b) the observed PSO kinetic rate constant of the $CaCO_3$ homogeneous nucleation.

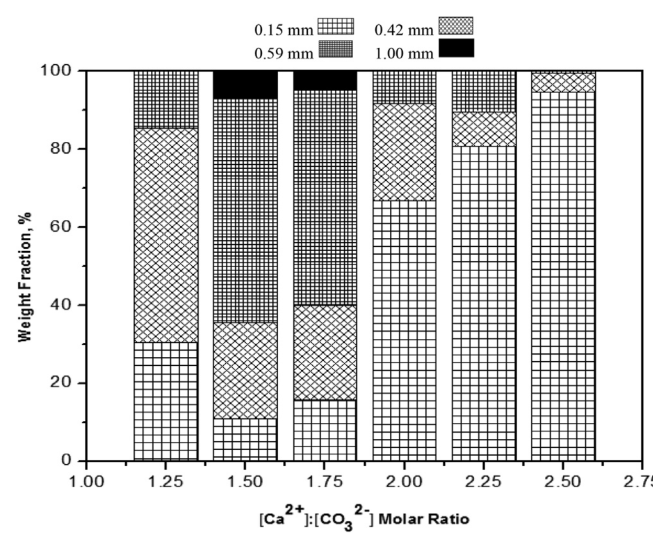

Fig. 4. Particle size distribution of the obtained granules at varying $[Ca^{2+}]/[CO_3{}^{2-}]$ levels.

shown in Eqs. (10)–(16) [37].

$$H^+ + HCO_3^- \leftrightarrow CO_2(aq) \quad \log K_{eq} = 6.341 \tag{10}$$

$$HCO_3^- \leftrightarrow H^+ + CO_3^{2-} \quad \log K_{eq} = -10.325 \tag{11}$$

$$Ca^{2+} + HCO_3^- \leftrightarrow H^+ + CaCO_3(aq) \quad \log K_{eq} = -7.009 \tag{12}$$

$$Ca^{2+} + HCO_3^- \leftrightarrow CaHCO_3 \quad \log K_{eq} = -0.653 \tag{13}$$

$$Ca^{2+} + H^+ \leftrightarrow CaOH \quad \log K_{eq} = -12.85 \tag{14}$$

$$- H^+ \leftrightarrow OH^- \quad \log K_{eq} = -13.991 \tag{15}$$

$$Ca^{2+} + CO_3^- \leftrightarrow CaCO_3(s) \tag{16}$$

The major ions monitored were Ca^{2+} and $CO_3{}^{2-}$ from the solutions of $Ca(OH)_2$ and K_2CO_3, respectively. However, it cannot be neglected that the presence of other ions could affect the granulation of $CaCO_3$ in the FBR. Other conditions could also affect the reaction, nucleation and granulation in which it should be considered and monitored throughout the investigation of the $CaCO_3$ granulation kinetics. Aside from the calcium precipitant dosage, pH is also an important parameter in identifying the dominant ions (bicarbonate, carbonate or hydroxide) in the system [38]. The best pH condition in the crystallization of $CaCO_3$ in the FBR through the homogeneous granulation was found to be between 10 and 11 [10]. At this pH, the dominant ions present in the system were carbonate. Thus, a higher efficiency in the $CaCO_3$ granulation is expected.

3.2. $CaCO_3$ homogeneous granulation

The amount of calcium precipitant dosage can significantly affect the $CaCO_3$ granulation performance in the FBHG process. The molar

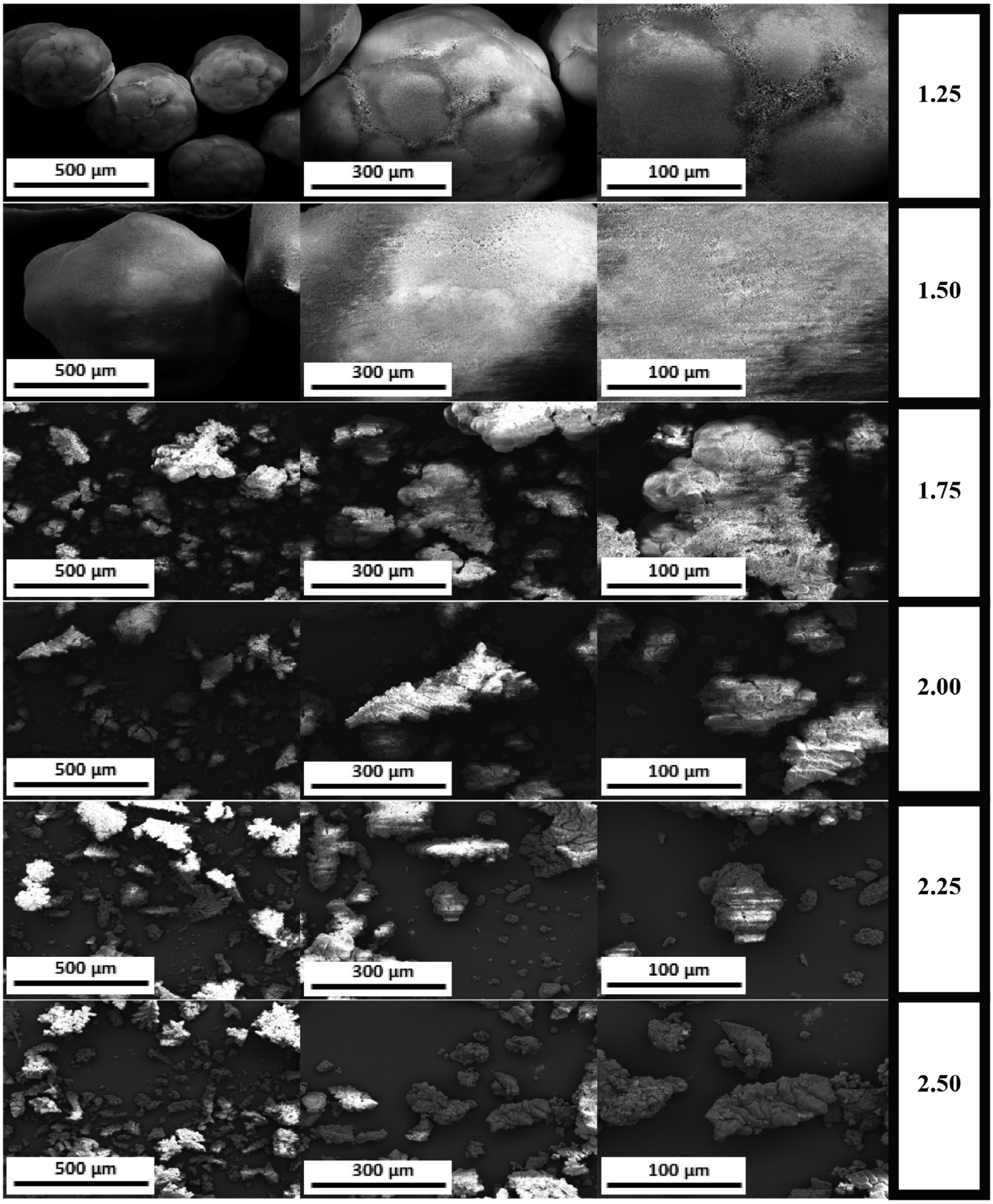

Fig. 5. SEM images of $CaCO_3$ granulated through the FBHG process at varying $[Ca^{2+}]/[CO_3^{2-}]$ ratio.

ratio parameter is essential due to being able to regulate the amount of calcium precipitant that could react with the carbonate ions to granulate $CaCO_3$. Increasing the calcium concentration increases the supersaturation state of the solution to granulate $CaCO_3$ that results to a higher removal and granulation [10]. $CaCO_3$ granulation in the FBR was conducted at an operating pH of 10 ± 0.2, $[CO_3^{2-}]_{in}$ of 10 mM, Q_T of 60 mL min^{-1} and at the varying $[Ca^{2+}]/[CO_3^{2-}]$ condition of 1.25, 1.50, 1.75, 2.00, 2.25 and 2.50. In each of the experimental conditions, the efficiencies in FBHG process had an increasing trend in the time series that became stable when the granules formed reached the uppermost part of the reaction region [39]. The average efficiencies were computed from the average of the stable readings of every 24 h in the experimental condition.

As observed in Fig. 3(a), a higher $[Ca^{2+}]/[CO_3^{2-}]$ condition increases the total carbonate removal efficiency. This is due to more $[Ca^{2+}]$ ions that would react with $[CO_3^{2-}]$ ions leading towards a greater potential to remove $[CO_3^{2-}]$ ions from the system and a faster chemical reaction [13]. However, increasing the $[Ca^{2+}]/[CO_3^{2-}]$ condition too high can cause a decrease in the carbonate granulation efficiency that indicates more fines and sludge present in the effluent region. Based on Fig. 3(b), a quadratic relationship is shown between the PSO kinetic rate constant and the $[Ca^{2+}]/[CO_3^{2-}]$ parameter. As the $[Ca^{2+}]/[CO_3^{2-}]$ condition increase, the rate constant reached its peak (maximum) and caused a decline in the rate of chemical reaction of the $CaCO_3$ granulation when the $[Ca^{2+}]/[CO_3^{2-}]$ level is too high. At a large quantity of $Ca(OH)_2$ precipitant, more OH^- in the system can

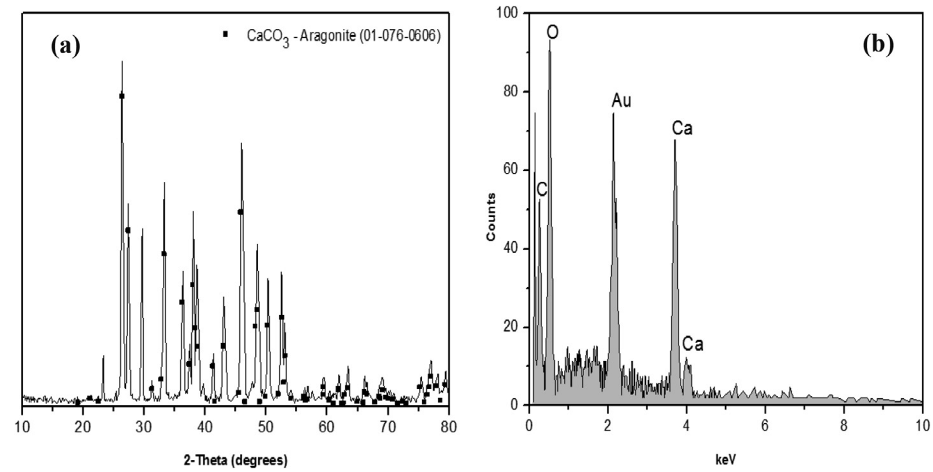

Fig. 6. (a) X-ray diffraction pattern and (B) energy-dispersive X-ray spectrum of the $CaCO_3$ granules precipitated in the FBHG process at a $[Ca^{2+}]/[CO_3{}^{2-}]$ ratio of 1.50.

affect the rate of $CaCO_3$ granulation by co-precipitating $Ca(OH)_2$ that causes the production of slurry sludge [40].

The particle size distribution in each experimental run was also done through the calculation of $[Carbonate]_{WF}$ using W_t and W_{ms}. As shown in Fig. 4, a further increase in the $[Ca^{2+}]/[CO_3{}^{2-}]$ condition produces more 0.15 mm granules that were lighter and smaller. This supports the decreased in the carbonate granulation efficiency. At the $[Ca^{2+}]/[CO_3{}^{2-}]$ levels of 1.50 and 1.75, an ideal particle size distribution trend was observed. This is due to the production of larger granules. Once the nuclei were produced in the homogeneous nucleation, the particles continued to flocculate and granulate into a bigger sized granules. Larger granules imply more $CaCO_3$ that was granulated and remained inside the reactor. The particle size distribution trend leading towards the production of bigger granules provided a variety of sizes that could be granulated in the FBR through the homogeneous granulation process [41]. Both the conditions were able to produce 1 mm to 2 mm (by diameter) granules. However, a higher weight fraction percentage of it (7%) was achieved at a $[Ca^{2+}]/[CO_3{}^{2-}]$ level of 1.50. Economically, the $[Ca^{2+}]/[CO_3{}^{2-}]$ condition of 1.50 was also preferred to be used than the 1.75. This is due to utilizing a lesser amount of precipitant that implies fewer chemical input and expense. Other $[Ca^{2+}]/[CO_3{}^{2-}]$ conditions showed the production of finer granule sizes that indicated the homogeneous nucleation as the dominant mechanism in the system. Moreover, there was a slow granulation mechanism due to reaching a high supersaturation state that increases the production of fines [12].

Obtaining high removal and granulation efficiencies were necessary, especially in the treatment and recovery steps. This could be done by adding a high precipitant dose in the system. However, for industrial purposes and commercialization, the interest was more on the production of high purity and larger granule sizes [39]. Therefore, the use of $[Ca^{2+}]/[CO_3{}^{2-}]$ at 1.50 was defined as the best operational condition in the $CaCO_3$ granulation through FBHG process.

3.3. $CaCO_3$ granule characterization

The physical characteristics of the biggest $CaCO_3$ granules produced in different $[Ca^{2+}]/[CO_3{}^{2-}]$ conditions were analyzed using the SEM to determine the surface morphology and shape of the granules. Fig. 5 showed the SEM images of the $CaCO_3$ granules produced by varying the $[Ca^{2+}]/[CO_3{}^{2-}]$, at three different magnifications. As shown in the figure, $[Ca^{2+}]/[CO_3{}^{2-}]$ has a significant effect on the appearance of the granules in terms of its surface morphology and the shape of the $CaCO_3$ granules. At the $[Ca^{2+}]/[CO_3{}^{2-}]$ levels of 1.25 and 1.50, the shape of the granules was subrounded. However, the granules at a $[Ca^{2+}]/[CO_3{}^{2-}]$ level of 1.50 were bigger in size, not easy to break, and with a smooth surface [10]. The hardness of the granules at this condition was due to the compact agglomeration of particles during granulation that can be observed in the SEM images. While a $[Ca^{2+}]/[CO_3{}^{2-}]$ level of 1.25 exhibited a slower granulation mechanism as supported by the hollows on the surface and smaller size granules produced at this condition. A further increase in the $[Ca^{2+}]/[CO_3{}^{2-}]$ condition resulted in a decline in the production of bigger size granules that conversely increases the production of fine granules. Even though higher $[Ca^{2+}]/[CO_3{}^{2-}]$ levels has led to a higher efficiency of $[Carbonate]_{TR}$, the granules produced at extreme calcium precipitant dosages had the physical characteristics of irregular shapes and rough surfaces. The $[Ca^{2+}]/[CO_3{}^{2-}]$ level greater than 1.50 can produce bigger granules at a faster growth rate as observed inside the FBR. However, during collection and drying, the granules tend to break in powdered form. A $[Ca^{2+}]/[CO_3{}^{2-}]$ condition that is too high also resulted to clogging in the inlets of the reactor and causes an unclear effluent. This is due to the production of sludge caused by the precipitation of hydroxide and the additional hydroxide content derived from the calcium hydroxide precipitant [40].

The XRD pattern depicted in Fig. 6(a) of the resulting granules exhibited the characteristic of aragonite, with the line graph fitted into the aragonite pattern at 2-Theta of major peaks of 26.4°, 29.7°, 33.3°, 36.0°, 38.1°, 43.0°, 46.0°, 48.5°, 50.3° and 52.5°. Since the reaction time in every experiment was 168 h, aragonite was formed. This was attributed to the longer reaction time that favored the formation of $CaCO_3$-aragonite granules [42].

The chemical composition of the $CaCO_3$ granules analyzed by the EDX as shown in Fig. 6(b) revealed the presence of calcium, carbon and oxygen, which were the elements in the $CaCO_3$ compound. The analysis proved a high purity of $CaCO_3$-aragonite granule produced by $CaCO_3$ precipitation through the FBHG process, with no trace amounts of other elements. The AuM detected and shown in the figure stands for the contribution of the X-ray given off as the electron to M shells [43].

4. Conclusions

This research study investigated the kinetics of $CaCO_3$ granulation in the FBR during the first 24 h of the experiment. The following was concluded based on the experimental results: (a) The kinetics of $CaCO_3$ granulation through the FBHG process fitted in the PSO model. This means that the mechanism followed the assumption of the occurrence of chemical sorption that instigated nucleation and granulation. (b) The best $[Ca^{2+}]/[CO_3{}^{2-}]$ level is at 1.50 due to the formation of larger granule sizes. (c) Low $[Ca^{2+}]/[CO_3{}^{2-}]$ levels leads to smaller and hollow surfaces in the granules, while high $[Ca^{2+}]/[CO_3^{2-}]$ conditions promotes the production of fine granules due to an excess amount hydroxide (precipitant). (d) The $CaCO_3$ granules were confirmed to have the characteristic of aragonite and the elements of Ca, C and O based on the XRD and EDX analyses, respectively. This proves the generation of a high purity $CaCO_3$-aragonite granule produced in the $CaCO_3$ granulation through the FBHG process. Higher removal and granulation efficiencies were obtained. Moreover, the products attained less moisture content, high purity and bigger $CaCO_3$ granules. The research gap of a lack of kinetic analysis in the aspect of $CaCO_3$ granulation has been properly addressed. This research paper showed an innovative conversion of K_2CO_3 (as the source of CO_2) to $CaCO_3$ granules for the possible application of carbon capture, utilization and storage in future works. Furthermore, potential research directions in continuation of this study can include the variations of pH, upflow velocity, bed hydrodynamics and the presence of other ions to better understand the utilization of FBHG process prior to industrial applications.

Declaration of Competing Interest

The authors declare that they have no known competing financial interests or personal relationships that could have appeared to influence the work reported in this paper

Acknowledgements

The authors would like to thank the Ministry of Science and Technology, Taiwan (Contract No. MOST-102-2221-E-041-001-MY3) and the National Research Foundation of Korea through the Ministry of Education (No. 2016R1A6A1A03012812) for providing financial support for this research undertaking.

References

[1] T. Oiso, S. Yamanaka, Template-free synthesis and particle size control of mesoporous calcium carbonate, Adv. Powder Technol. 29 (2018) 606–610, https://doi.org/10.1016/j.apt.2017.12.001.
[2] S. Teir, S. Eloneva, R. Zevenhoven, Production of precipitated calcium carbonate from calcium silicates and carbon dioxide, Energy Convers. Manage. 46 (2005) 2954–2979, https://doi.org/10.1016/j.enconman.2005.02.009.
[3] R. Aldaco, A. Garea, A. Irabien, Calcium fluoride recovery from fluoride wastewater in a fluidized bed reactor, Water Res. 41 (2007) 810–818, https://doi.org/10.1016/j.watres.2006.11.040.
[4] C.Y. Tai, P.C. Chen, T.M. Tsao, Growth kinetics of CaF2 in a pH-stat fluidized-bed crystallizer, J. Cryst. Growth. 290 (2006) 576–584, https://doi.org/10.1016/j.jcrysgro.2006.02.036.
[5] C.S. Chen, Y.J. Shih, Y.H. Huang, Remediation of lead (Pb(II)) wastewater through recovery of lead carbonate in a fluidized-bed homogeneous crystallization (FBHC) system, Chem. Eng. J. 279 (2015) 120–128, https://doi.org/10.1016/j.cej.2015.05.013.
[6] Z. Wei, A review of techniques for the process intensification of fluidized bed reactors, Chinese J. Chem. Eng. 17 (2009) 688–702, https://doi.org/10.1016/S1004-9541(08)60264-5.
[7] A.F.M. Salcedo, F.C.J. Ballesteros, M.-C. Lu, Recovery of nickel from industrial wastewater by homogeneous fluidized-bed granulation: effects of influent nickel concentration, CO3: Ni ratio and pH of the precipitant, Proc. 14th Int. Conf. Environ. Sci. Technol. 2015, pp. 1–5.
[8] A.C. Vilando, A.R. Caparanga, M.-C. Lu, Enhanced recovery of aluminum from wastewater using a fluidized bed homogeneously dispersed granular reactor, Chemosphere 223 (2019) 330–341, https://doi.org/10.1016/j.chemosphere.2019.02.086.
[9] K.A.A. Tiangco, M.D.G. de Luna, A.C. Vilando, M.C. Lu, Removal and recovery of calcium from aqueous solutions by fluidized-bed homogeneous crystallization, Process Saf. Environ. Prot. 128 (2019) 307–315, https://doi.org/10.1016/j.psep.2019.06.007.
[10] N.N.N. Mahasti, Y.J. Shih, X.T. Vu, Y.H. Huang, Removal of calcium hardness from solution by fluidized-bed homogeneous crystallization (FBHC) process, J. Taiwan Inst. Chem. Eng. 78 (2017) 378–385, https://doi.org/10.1016/j.jtice.2017.06.040.
[11] K. Lertratwattana, P. Kemacheevakul, S. Garcia-Segura, M.C. Lu, Recovery of copper salts by fluidized-bed homogeneous granulation process: high selectivity on malachite crystallization, Hydrometallurgy 186 (2019) 66–72, https://doi.org/10.1016/j.hydromet.2019.03.015.
[12] F.C. Ballesteros, A.F.S. Salcedo, A.C. Vilando, Y.H. Huang, M.C. Lu, Removal of nickel by homogeneous granulation in a fluidized-bed reactor, Chemosphere 164 (2016) 59–67, https://doi.org/10.1016/j.chemosphere.2016.08.081.
[13] H.P.R. Guevara, F.C. Ballesteros, A.C. Vilando, M.D.G. de Luna, M.C. Lu, Recovery of oxalate from bauxite wastewater using fluidized-bed homogeneous granulation process, J. Cleaner Prod. 154 (2017) 130–138, https://doi.org/10.1016/j.jclepro.2017.03.172.
[14] R.R. Pahunang, F.C. Ballesteros, M.D.G. de Luna, A.C. Vilando, M.C. Lu, Optimum recovery of phosphate from simulated wastewater by unseeded fluidized-bed crystallization process, Sep. Purif. Technol. 212 (2019) 783–790, https://doi.org/10.1016/j.seppur.2018.11.087.
[15] N. Udomkitthaweewat, J. Anotai, A.E.S. Choi, M.C. Lu, Removal of zinc based on a screw manufacturing plant wastewater by fluidized-bed homogeneous granulation process, J. Cleaner Prod. 230 (2019) 1276–1286, https://doi.org/10.1016/j.jclepro.2019.05.192.
[16] M. Kim, J. Na, S. Park, J.-H. Park, C. Han, Modeling and validation of a pilot-scale aqueous mineral carbonation reactor for carbon capture using computational fluid dynamics, Chem. Eng. Sci. 177 (2018) 301–312, https://doi.org/10.1016/j.ces.2017.11.033.
[17] A. Torabi, M. Kazemeini, M. Fattahi, Developing a mathematical model for the oxidative dehydrogenation of propane in a fluidized bed reactor, Asia-Pacific J. Chem. Eng. 11 (2016) 448–459, https://doi.org/10.1002/apj.1966.
[18] B. Khadem-Hamedani, S. Yaghmaei, M. Fattahi, S. Mashayekhan, S.M. Hosseini-Ardali, Mathematical modeling of a slurry bubble column reactor for hydrodesulfurization of diesel fuel: single- and two-bubble configurations, Chem. Eng. Res. Des. 100 (2015) 362–376, https://doi.org/10.1016/j.cherd.2015.05.023.
[19] B. Barghi, M. Fattahi, F. Khorasheh, The modeling of kinetics and catalyst deactivation in propane dehydrogenation over Pt-Sn/γ-Al2O3 in presence of water as an oxygenated additive, Pet. Sci. Technol. 32 (2014) 1139–1149, https://doi.org/10.1080/10916466.2011.631071.
[20] A. Samavati, M. Fattahi, F. Khorasheh, Modeling of Pt-Sn/γ-Al2O3 deactivation in propane dehydrogenation with oxygenated additives, Korean J. Chem. Eng. 30 (2013) 55–61, https://doi.org/10.1007/s11814-012-0095-z.
[21] M. Fattahi, M. Kazemeini, F. Khorasheh, A. Darvishi, A.M. Rashidi, Fixed-bed multitubular reactors for oxidative dehydrogenation in ethylene process, Chem. Eng. Technol. 36 (2013) 1691–1700, https://doi.org/10.1002/ceat.201300148.
[22] B. Ohs, M. Krödel, M. Wessling, Adsorption of carbon dioxide on solid amine-functionalized sorbents: a dual kinetic model, Sep. Purif. Technol. 204 (2018) 13–20, https://doi.org/10.1016/j.seppur.2018.04.009.
[23] A. Heydari-Gorji, A. Sayari, CO2 capture on polyethylenimine-impregnated hydrophobic mesoporous silica: experimental and kinetic modeling, Chem. Eng. J. 173 (2011) 72–79, https://doi.org/10.1016/j.cej.2011.07.038.
[24] M.M. Seckler, S.L. Bruinsma, G.M. Rosmalen, Calcium phosphate precipitation in a fluidized bed in relation to process conditions: a black box approach, Water Res. 30 (1996) 1677–1685, https://doi.org/10.1016/0043-1354(96)00043-7.
[25] A.F.M. Salcedo, F.C. Ballesteros, A.C. Vilando, M.C. Lu, Nickel recovery from synthetic Watts bath electroplating wastewater by homogeneous fluidized bed granulation process, Sep. Purif. Technol. 169 (2016) 128–136, https://doi.org/10.1016/j.seppur.2016.06.010.
[26] N. Smirnova, M.S. Demyan, F. Rasche, G. Cadisch, T. Müller, Calibration of CO < sub > 2 < /sub > trapping in alkaline solutions during soil incubation at varying temperatures using a respicond VI, Open J. Soil Sci. 04 (2014) 161–167, https://doi.org/10.4236/ojss.2014.45019.
[27] M.-R. Yoo, S.-J. Han, J.-Y. Shin, J.-H. Wee, A study on carbon dioxide capture performance of KOH aqueous solution via chemical absorption, J. Korean Soc. Environ. Eng. 34 (2012) 55–62, https://doi.org/10.4491/ksee.2012.34.1.055.
[28] K.S. Rybacki, 2010. Calcium carbonate precipitation mechanisms and geochemical analysis of particulate material found within the waters of Maramec Spring, St. James, Missouri, 47.
[29] K.V. Kumar, Linear and non-linear regression analysis for the sorption kinetics of methylene blue onto activated carbon, J. Hazard. Mater. 137 (2006) 1538–1544, https://doi.org/10.1016/j.jhazmat.2006.04.036.
[30] B. Liu, X. Luo, H. Gao, R. Idem, P. Tontiwachwuthikul, W. Olson, Z. Liang, Reaction kinetics of the absorption of carbon dioxide (CO2) in aqueous solutions of sterically hindered secondary alkanolamines using the stopped-flow technique, Chem. Eng. Sci. 170 (2017) 16–25, https://doi.org/10.1016/j.ces.2017.02.044.
[31] D. Tiwari, H. Bhunia, P.K. Bajpai, Adsorption of CO2 on KOH activated, N-enriched carbon derived from urea formaldehyde resin: kinetics, isotherm and thermodynamic studies, Appl. Surf. Sci. 439 (2018) 760–771, https://doi.org/10.1016/j.apsusc.2017.12.203.
[32] J. Singh, H. Bhunia, S. Basu, CO2 adsorption on oxygen enriched porous carbon monoliths: kinetics, isotherm and thermodynamic studies, J. Ind. Eng. Chem. 60 (2018) 321–332, https://doi.org/10.1016/j.jiec.2017.11.018.
[33] H. Liu, M. Li, R. Idem, P. (PT) Tontiwachwuthikul, Z. Liang, Analysis of solubility, absorption heat and kinetics of CO2 absorption into 1-(2-hydroxyethyl)pyrrolidine solvent, Chem. Eng. Sci. 162 (2017) 120–130, https://doi.org/10.1016/j.ces.2016.12.070.
[34] V. Fierro, V. Torné-Fernández, D. Montané, A. Celzard, Adsorption of phenol onto activated carbons having different textural and surface properties, Microporous Mesoporous Mater. 111 (2008) 276–284, https://doi.org/10.1016/j.micromeso.2007.08.002.
[35] M. Yildirim, H. Akarsu, Kinetics of calcium carbonate (CaCO3) precipitation from a Icel-Yavca dolomite leach solution by a gas (carbon dioxide)/liquid reaction, Helv. Chim. Acta. 92 (2009) 502–513, https://doi.org/10.1002/hlca.200800303.
[36] Y.S. Ho, Review of second-order models for adsorption systems, J. Hazard. Mater. 136 (2006) 681–689, https://doi.org/10.1016/j.jhazmat.2005.12.043.
[37] T. Gebrehiwet, L. Guo, D. Fox, H. Huang, Y. Fujita, R. Smith, J. Henriksen, G. Redden, Precipitation of calcium carbonate and calcium phosphate under diffusion controlled mixing, Appl. Geochem. 46 (2014) 43–56, https://doi.org/10.

1016/j.apgeochem.2014.04.005.
[38] D.A. Skoog, D.M. West, Fundamentals of analytical chemistry, J. Chem. Educ. 40 (1963) 614, https://doi.org/10.1021/ed040p614.2.
[39] P.S. Caddarao, S. Garcia-Segura, F.C. Ballesteros, Y.H. Huang, M.C. Lu, Phosphorous recovery by means of fluidized bed homogeneous crystallization of calcium phosphate. Influence of operational variables and electrolytes on brushite homogeneous crystallization, J. Taiwan Inst. Chem. Eng. 83 (2018) 124–132, https://doi.org/10.1016/j.jtice.2017.12.009.
[40] M.S. Oncel, A. Muhcu, E. Demirbas, M. Kobya, A comparative study of chemical precipitation and electrocoagulation for treatment of coal acid drainage wastewater, J. Environ. Chem. Eng. 1 (2013) 989–995, https://doi.org/10.1016/j.jece.2013.08.008.
[41] Y. Liu, G. Lan, P. Zeng, Size-dependent calcium carbonate precipitation induced microbiologically in aerobic granules, Chem. Eng. J. (2015), https://doi.org/10.1016/j.cej. 2015.10.020.
[42] C. Ramakrishna, T. Thenepalli, J.H. Huh, J.W. Ahn, Preparation of needle like aragonite precipitated calcium carbonate (PCC) from dolomite by carbonation method, J. Korean Ceram. Soc. 53 (2016) 7–12, https://doi.org/10.4191/kcers.2016.53.1.7.
[43] Y.S. Al Jabbari, X. Barmpagadaki, S.M. Al Taweel, S. Zinelis, The effect of simulating porcelain firing on the elemental composition, microstructure, and mechanical properties of electroformed gold restorations, J. Dental Sci. 11 (3) (2016) 266–271, https://doi.org/10.1016/j.jds.2016.03.001.